Research

Check for updates

Author for correspondence:
Guido Boffetta
e-mail: guido.boffetta@unito.it

Dimensional effects in Rayleigh–Taylor mixing

Guido Boffetta and Stefano Musacchio

Department of Physics and INFN, via P. Giuria 1, 10125 Torino, Italy

GB, 0000-0002-2534-7751

We study the effects of dimensional confinement on the evolution of incompressible Rayleigh–Taylor mixing both in a bulk flow and in porous media by means of numerical simulations of the transport equations. In both cases, the confinement to two-dimensional flow accelerates the mixing process and increases the speed of the mixing layer. Dimensional confinement also produces stronger correlations between the density and the velocity fields affecting the efficiency of the mass transfer, quantified by the dependence of the Nusselt number on the Rayleigh number.

This article is part of the theme issue 'Scaling the turbulence edifice (part 2)'.

1. Introduction

Space dimensionality affects many dynamical and statistical properties of flows. Uriel Frisch pioneered the studies of dimensional effects in fluid dynamics, by investigating the phenomenology of turbulent flows in fractal dimensions [1,2] and in infinite dimensions [3]. In the case of turbulent flows at high Reynolds number, the direction of the turbulent cascade of kinetic energy depends on the dimension of the space. In three dimensions, the energy is transferred from large to small scales (direct cascade), while in two dimensions the direction of the energy transfer is inverted from small to large scales (inverse cascade) [4–6]. Numerical [7,8] and experimental [9,10] studies of turbulent flows confined in a thin layer have observed the transition between the two-dimensional and three-dimensional phenomenology, with an intermediate state of coexistence of the two cascades. (for a recent review of this subject, see [11]).

In this work, we investigate the role of the space dimensionality in the Rayleigh–Taylor (RT) convection. RT mixing is produced by a well-known instability at the interface of two fluids with different density,

initially at rest, in the presence of a relative acceleration. The instability eventually develops in a nonlinear phase producing a mixing layer (ML), characterized by density and velocity fluctuations, which grows in time [12,13].

The study of RT turbulence is motivated by a wide spectrum of applications, including supernova explosion [14], plasma physics [15], laser-matter interaction [16] and inertial confinement fusion [17]. In view of these applications, RT is usually studied in bulk fluids at low viscosity, in which the velocity of the rising and falling plumes grows in time as t and the width of the ML follows an accelerated growth as t^2. Inside the ML, the density field is mixed by the flow up to small scales, at which molecular diffusivity becomes dominant.

The RT mixing has also been extensively studied in porous media. In this case, the linear instability [18] develops in a ML that grows dimensionally as t, as a consequence of the balance between the gravity force and the viscous friction with the porous medium, which produces a constant asymptotic velocity. Recently, experimental and numerical studies of porous RT mixing have been done both in two dimensions [19,20] and in three dimensions [21,22]. The increasing interest for the RT mixing in porous media is motivated by its applications in CO_2 sequestration in saline aquifers. Dissolution of carbon dioxide in the aqueous phase increases its density and induces a buoyancy-driven instability that accelerates the process of CO_2 sequestration into the bulk of the aquifer [23,24].

The phenomenology of RT turbulence in bulk flow is strongly affected by the dimensionality [13]. In three dimensions, the buoyancy force originates a direct cascade of kinetic energy inside the ML with Kolmogorov–Obukhov scaling laws for the velocity and density fluctuations [25,26]. In two dimensions, the balance between the inverse energy cascade and the buoyancy produces the Bolgiano–Obukhov phenomenology [25,27,28]. In the case of RT in a thin layer, the confining scale becomes the Bolgiano scale of the flow that separates the different scaling regimes [28].

On the contrary, for the case of RT in porous media, there is no theoretical reason to expect that the space dimensionality affects the scaling properties of the system, because the dynamics is completely governed by the balance between gravity force and viscosity and the inertial effects are absent. Indeed similar dimensional scaling laws have been observed both in two-dimensional [19,20] and in three-dimensional [21,22] studies of porous RT mixing. Nonetheless, recent numerical studies have revealed a significant quantitative difference between the RT mixing in two dimensions and in three dimensions [22] with a sharp transition between the two regimes as the lateral extension narrows [29].

The aim of this paper is to present in a systematic way the role of space dimensionality in RT mixing, both in bulk flow and porous media. For this purpose, we present a direct comparison of the results of numerical simulations in two dimensions and in three dimensions of the RT system in bulk flow, accompanied by a review of recent numerical results of RT mixing in porous media [22].

We focus on the global properties of the flow inside the ML, the temporal evolution of the mean density profiles, the speed of the development of the ML, the efficiency of mixing inside the ML and the transport of mass quantified by the Nusselt number. We show that, in general, the ML in two-dimensional geometry grows faster and with larger fluctuations than in three-dimensional, both for bulk and for porous flows. Also the transfer of heat is larger in two-dimensional geometry, as a result of stronger correlations between the density fluctuations and the vertical velocity.

2. Models and methods

We consider the RT configuration in a three-dimensional (x, y, z) or two-dimensional (x, z) domain with gravity pointing downwards $\mathbf{g} = -g\hat{\mathbf{k}}$. The density field is written as $\rho(\mathbf{x}, t) = \rho_0(1 + \theta(\mathbf{x}, t))$ with an initial unstable vertical density profile, $\theta(\mathbf{x}, 0) = \text{sgn}(z)\Delta\theta/2$ such that the Atwood number is $A = \Delta\theta/2$.

Table 1. Summary of the simulations. N_x, N_y and N_z are the resolutions in the three directions of sizes L_x, L_y and L_z. N_R is the number of independent realizations. NS refers to the simulations of (2.1)–(2.3), D to those of (2.2) and (2.3) in two-dimensional and three-dimensional geometries.

	N_x	N_y	N_z	L_x	L_y	L_z	N_R
NS3D	1024	1024	2048	4π	4π	8π	2
NS2D	1024	1	2048	4π	0	8π	20
D3D	2048	2048	8192	2π	2π	8π	1
D2D	2048	1	8192	2π	0	8π	15

In the limit of small A the Boussinesq approximation for an incompressible velocity field holds and the dynamics for a bulk flow is governed by the (Boussinesq)–Navier–Stokes equations

$$\rho_0(\partial_t \mathbf{u} + \mathbf{u} \cdot \nabla \mathbf{u}) = -\nabla p + \mu \nabla^2 \mathbf{u} + \mathbf{g}\rho_0\theta, \tag{2.1}$$

where μ is the viscosity.

In the case of a flow in a porous media, we will consider the (Boussinesq)–Darcy model, which can be obtained from (2.1) by neglecting the acceleration terms on the lhs and by replacing the Laplacian in the viscosity term with an (isotropic) permeability κ and the porosity ϕ of the medium

$$\mathbf{u} = \frac{\kappa}{\mu\phi}(-\nabla p + \mathbf{g}\rho_0\theta). \tag{2.2}$$

In both cases, the field of density fluctuations evolves according to the advection–diffusion equation

$$\partial_t\theta + \mathbf{u} \cdot \nabla\theta = D\nabla^2\theta, \tag{2.3}$$

where D is the diffusion coefficient.

We performed direct numerical simulations of the systems (2.1)–(2.3), (2.2) and (2.3) by means of a fully parallel, 2/3 dealiased, pseudo-spectral code in a triply periodic domain of sizes $L_x \times L_y \times L_z$ ($L_x \times L_z$ in two dimensions) with uniform grid at resolution $N_x \times N_y \times N_z$. Without loss of generality, in the simulations the reference density is set to $\rho_0 = 1$. The initial condition is the unstable jump at $z = 0$ for the density field and vanishing initial velocity. In order to trigger the instability, a small white noise perturbation is added to the initial density field around the interface at $z = 0$. A zero-velocity mask is imposed at the stable density jump at $z = \pm L_z/2$. In order to improve the statistical accuracy, simulation results have been averaged over a set of N_R independent realizations of the initial random perturbations. While in three dimensions the statistical convergence of the results benefits from the average over the horizontal (x, y) planes, in two dimensions it is necessary to perform several independent realizations to achieve convergent results. A summary of simulation parameters is given by table 1.

For the discussion of the results in the next section, we will use two different spatial averages: the three-dimensional (or two-dimensional) average over the whole volume $\langle \cdots \rangle \equiv (1/L_xL_yL_z) \iiint \cdots \, \mathrm{d}x \, \mathrm{d}y \, \mathrm{d}z$ (and the analogous in two dimensions) and the profile average over the planes (lines) normal to gravity $\overline{\cdots} \equiv (1/L_xL_y) \iint \cdots \, \mathrm{d}x \, \mathrm{d}y$ (and the analogous in two dimensions). The average over the N_R realizations is implied for all the results.

3. Results

The effects of the space dimensionality on the RT mixing, as well as the different dynamics of the NS and Darcy systems, are already evident at a qualitative level by comparing the vertical sections of the density fields obtained in the late stage of the simulations, shown in figure 1. In the case of bulk flow, the convective turbulent structures (usually called 'plumes') are very different in two dimensions and in three dimensions, reflecting the different scaling of the velocity and density
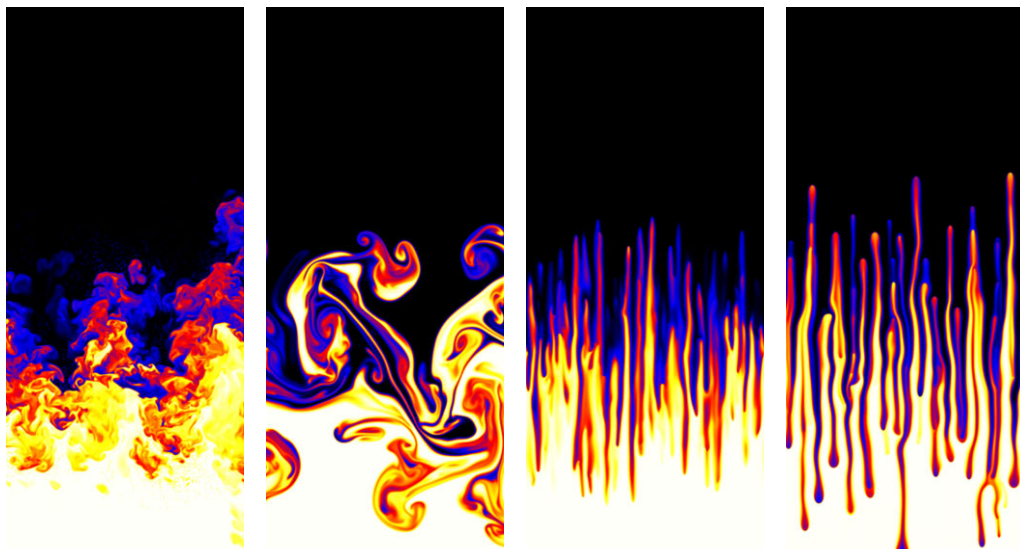
Figure 1. From left to right: vertical sections of the density field for a three-dimensional NS simulation, a two-dimensional NS simulation, both at time $t = 25$, and for a three-dimensional Darcy simulation and a two-dimensional Darcy simulation, both at time $t = 30$. White (black) represents light (heavy) fluid and gravity is in the vertical direction. (Online version in colour.)

fields. In particular, the inverse cascade with Bolgiano scaling produces the large scale structures observed in two dimensions. Nonetheless, both two-dimensional and three-dimensional density fields develop plumes with large horizontal and vertical scales that grow proportionally to the extension of the ML.

Conversely, the convective structures that appear in the Darcy convection are noticeably elongated (and hence are called 'fingers') and their aspect is very similar in two dimensions and in three dimensions. A common feature among the NS and Darcy cases is that the extension of the two-dimensional structures (plumes or fingers) is wider than in the corresponding three-dimensional case at the same time, as can be clearly appreciated in figure 1 for the Darcy case. Moreover, the three-dimensional structures are more blurred than their two-dimensional counterpart.

It is remarkable that despite the qualitative and quantitative difference between the convective structures of NS and Darcy RT systems, the mean density profiles $\overline{\theta}(z)$ are very similar. In both cases, they develop a quasi-linear profile $\overline{\rho}(z) \simeq \gamma(t)z$ in the ML, as shown in figure 2. Moreover, the two-dimensional profiles are broader than in the three-dimensional case. This provides a first indication that the mixing between the two reservoirs is faster in two dimensions than in three dimensions both for NS and Darcy dynamics. The latter result is surprising, since the dynamics of porous convection is not expected *a priori* to depend on the space dimensionality.

In order to better quantify this issue, we show in figure 3 the time evolution of the extension h of the ML for the two-dimensional and three-dimensional simulations. In general, the extension of the ML can be defined either in terms of global or local properties of the density profile. The simplest measure, used in the following, is based on the threshold value h at which $\overline{\theta}(z)$ reaches a fraction r of the maximum value, i.e. $\overline{\theta}(\pm h/2) = \pm r\Delta\theta/2$ [30]. Here, we use $r = 0.9$. In the NS cases, after an initial transient time t_0, we observe a quadratic growth of $h(t)$ that is consistent with
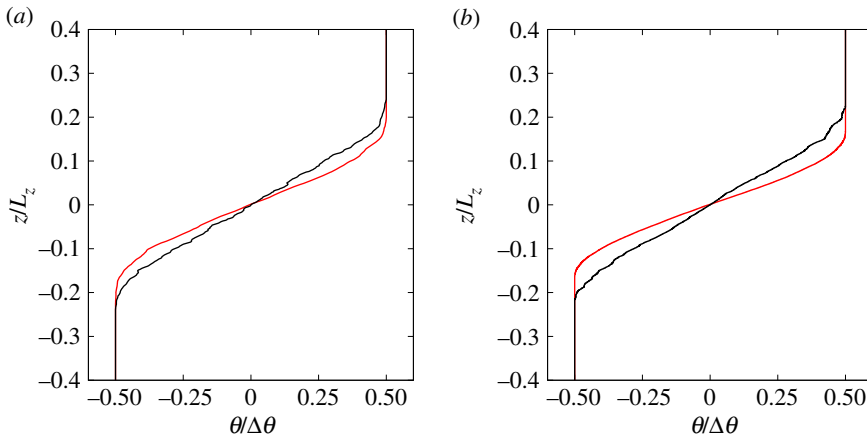
Figure 2. Mean density profiles $\overline{\theta}(z)$ for three-dimensional (red) and two-dimensional (black) NS simulations at time $t = 25$ (*a*) and for the Darcy simulations at time $t = 30$ (*b*), corresponding to the sections shown in figure 1. (Online version in colour.)
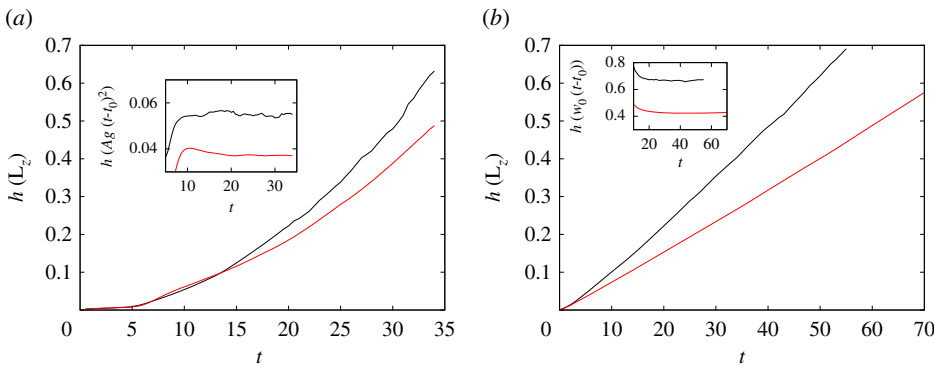

Figure 3. Temporal growth of the ML $h(t)$ for the three-dimensional (red) and the two-dimensional (black) flows for the NS (*a*) and Darcy (*b*) simulations. Inset: compensated plots $h/(Ag(t - t_0)^2)$ and $h/(w_0(t - t_0))$, which give the dimensionless constant α. (Online version in colour.)

the dimensional prediction $h(t) = \alpha Ag(t - t_0)^2$ both in two dimensions and three dimensions [13]. Nonetheless, we find that this growth is faster for the two-dimensional geometry corresponding to a dimensionless coefficient $\alpha_{\rm NS2D} \simeq 0.055$ larger than the coefficient $\alpha_{\rm NS3D} \simeq 0.037$ by about 57% (see the inset of figure 3, where we show the values of α obtained by compensating $h(t)$ with $Ag(t - t_0)^2$ with t_0 fitting parameter). We remark that we stop our analysis at the time $t = 35$ when the extension of the two-dimensional ML is still much smaller than the vertical extension L_z. This is because the horizontal correlation scale in two dimensions grows in time (approximatively proportional to h, as is evident from figure 1). Therefore, for large time the density field develops structure on the size of the horizontal scale L_x and the evolution is affected by finite size effects (we check the importance of these effects by comparing this case with simulations at $L_x = 2\pi$). As shown in figure 1, this limitation is less restrictive for the three-dimensional case, which develops correlations at smaller horizontal scale.

In the Darcy case, after an initial acceleration due to gravity forces, the fingers are expected to reach a constant velocity $w_0 = \kappa g\rho_0 \Delta\theta/\mu\phi$, determined by the balance between the gravity and the friction with the porous medium. The width of the ML is therefore expected to grow as $h(t) \sim t$. The dimensional scaling is confirmed by our results. Both in the two-dimensional and
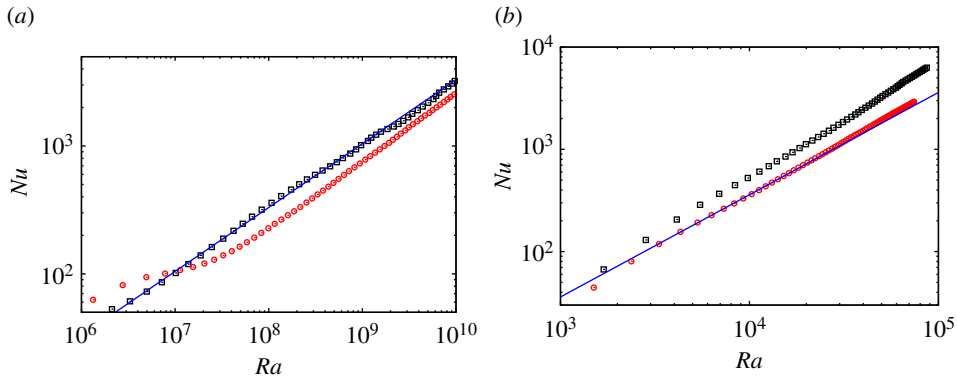
Figure 4. Nusselt number as a function of the Rayleigh number for the three-dimensional (red) and the two-dimensional (black) flows for the NS (*a*) and Darcy (*b*) simulations. The blue lines are the dimensional scaling $Nu \sim Ra^{1/2}$ (*a*) and $Nu \sim Ra$ (*b*). (Online version in colour.)

three-dimensional cases, after an initial transient t_0 we observe a linear growth of the ML $h(t) = \alpha w_0(t - t_0)$ (figure 3*a*). As in the NS case, the growth is faster in the two-dimensional geometry, with a coefficient $\alpha_{D2D} \simeq 0.67$ larger than the coefficient $\alpha_{D3D} \simeq 0.43$ by about 57% (see the inset of figure 3). Surprisingly, the ratio between the coefficients α_{D2D} and α_{D3D} in the Darcy case is very close to that of the NS coefficients.

The faster development of the ML in two-dimensional geometry is accompanied by an increase of the mass flux. The latter is quantified by the Nusselt number $Nu = \langle u_z \theta \rangle h/D\Delta\theta$, which is proportional to the correlation between the vertical velocity fields u_z and density field θ. In the absence of boundaries, the Nusselt number is expected to follow the dimensional scaling (the so-called 'ultimate state') as a function of the Rayleigh number, which in the case of bulk RT is defined as $Ra = \Delta\theta g h^3/\nu D$, (where $\nu = \mu/\rho_0$ is the kinematic viscosity), while in the Darcy case is $Ra = \Delta\theta g \kappa h/\nu D\phi = w_0 h/D$. In the NS case, the dimensional prediction for the growth of turbulent scales and velocities are $h \sim Agt^2$ and $u \sim Agt$, which gives $Nu \sim t^3 \sim Ra^{1/2}$. In the Darcy case, one has $h \sim w_0 t$ and $u \sim w_0$, which gives $Nu \sim t \sim Ra$. The results of our simulations are in agreement with the dimensional scaling, and they show that the values of Nu at given Ra (and therefore at fixed extension h of the ML) are always larger in two dimensions than in three dimensions (see figure 4). This indicates that in two-dimensional geometry the mass flux is more intense and correlation between the fields u_z and θ is stronger.

Besides the process of mixing between the two reservoirs, it is also interesting to investigate the effects of dimensionality on the mixing inside the mixing of the density fluctuations within the ML. A suitable measure of this process is given by the variance of the density fluctuations, defined as $\sigma^2(t) = \langle \overline{\theta^2}(z,t) - \overline{\theta}^2(z,t) \rangle_z$, where the average over the z direction is restricted to the ML $\langle \cdots \rangle_z \equiv (1/h) \int_{-h/2}^{+h/2} \cdots dz$. If the density field is completely mixed (as in the case of diffusive mixing), θ is constant over horizontal planes, i.e. $\theta(x, y, z) = \theta(z)$ and therefore $\sigma^2 = 0$. On the contrary, for a fully unmixed density, which assumes only the values $\pm\Delta\theta/2$, the variance attains the maximum value $\sigma_{max}^2 = \Delta\theta^2/4$. The time evolution of the variance is shown in figure 5. In the three-dimensional cases, at times $t > 10$ the variance reaches an almost constant value $(0.14 \pm 0.01)\sigma_{max}^2$ (for the NS3D case) and $(0.15 \pm 0.01)\sigma_{max}^2$ (for the D3D case). In the NS2D case an almost constant value $(0.32 \pm 0.01)\sigma_{max}^2$ is attained at times $t > 10$, while in the D2D case we observe a monotonic increase from $\sigma^2 = 0.24\sigma_{max}^2$ at time $t = 10$ to the final value $\sigma^2 = 0.30\sigma_{max}^2$ at time $t = 55$. Both in NS and Darcy simulations, the variance in two dimensions are always larger than in three dimensions, indicating that the density fluctuations are less mixed within the ML.

In the case of RT turbulence, it is possible to explain the dependence of the mixing properties on the dimensionality of the system in terms of the different scaling laws that are predicted in
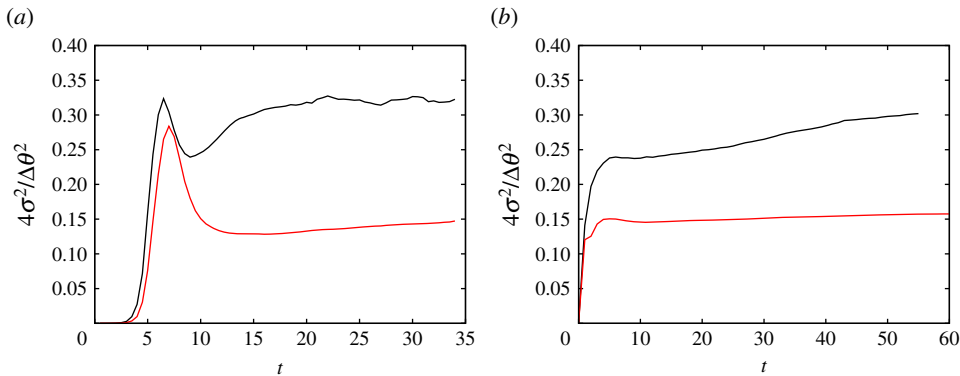
Figure 5. Temporal evolution of the variance of the density field for the three-dimensional (red) and the two-dimensional (black) flows for the NS (*a*) and Darcy (*b*) simulations. (Online version in colour.)

the two-dimensional and three-dimensional cascades [25]. In both cases, the growth of the ML $h \simeq Agt^2$ is produced by the conversion of the available potential energy $P = -g\langle z\theta \rangle$ into kinetic energy $E = \frac{1}{2}\langle \mathbf{u}^2 \rangle$. During this process, a fraction of the kinetic energy is dissipated by viscosity with a rate $\varepsilon = \nu\langle (\nabla \mathbf{u})^2 \rangle$ and the energy balance of the system reads

$$\frac{dE}{dt} = g\langle u_z \theta \rangle - \varepsilon = -\frac{dP}{dt} - Dg\Delta\theta - \varepsilon. \tag{3.1}$$

We remark that the dissipation rate of the potential energy due to the diffusivity $Dg\Delta\theta$ is almost negligible.

We briefly recall the different phenomenology of two-dimensional and three-dimensional RT turbulence (for further details see [13,25]). In three dimensions, the turbulent flow is driven by the buoyancy forces at large scales, while small-scale density fluctuations become passively transported at small scales. The scenario that emerges is a double direct cascade of both kinetic energy and density fluctuations inside the ML with Kolmogorov–Obukhov scaling laws [25]. In particular, the velocity fluctuations follow the Kolmogorov scaling $\delta u(\ell) \simeq \varepsilon(t)^{1/3}\ell^{1/3}$ with a viscous dissipation rate $\varepsilon(t) \simeq (Ag)^2 t$, while the density fluctuations follow the Obukhov scaling $\delta\theta(\ell) \simeq \varepsilon_\theta(t)^{1/2}\varepsilon(t)^{-1/6}\ell^{1/3}$ with density dissipation rate $\varepsilon_\theta(t) \simeq A^2/t$. Combining these scalings, one gets that the kinetic energy grows as $E \sim (\delta u(h))^2 \simeq (Agt)^2$. Therefore, the growth rate of the kinetic energy and the viscous dissipation rate follow the same temporal scaling $dE/dt \sim (Ag)^2 t \simeq \varepsilon$. The local Richardson number, which is defined as the ratio between the buoyancy force $g\delta\theta(\ell)$ and the inertial forces $(\delta u(\ell))^2/\ell$ at the scale ℓ, scales as $Ri(\ell) \simeq (\ell/h)^{2/3}$ and therefore vanishes at scales $\ell \ll h$, in agreement with the assumption that the buoyancy is negligible at small scales.

In two dimensions, the scenario is different because the turbulent flow induces an energy transfer towards large scales. Given that $Ri(\ell)$ grows with ℓ, the density fluctuations cannot be passively transported. In this case, the scale-by-scale balance between the buoyancy forces and inertial forces $g\delta\theta(\ell) \simeq (\delta u(\ell))^2/\ell$, accompanied by a direct cascade of density fluctuations, produces the Bolgiano–Obukhov phenomenology [25,27,28]. The scaling for the velocity fluctuations is $\delta u(\ell) = g^{2/5}\varepsilon_\theta(t)^{1/5}\ell^{3/5}$, while the density fluctuations scale as $\delta u(\ell) = g^{-1/5}\varepsilon_\theta(t)^{2/5}\ell^{1/5}$ where $\varepsilon_\theta(t) \sim A^2/t$ is the flux of the turbulent cascade of density fluctuations. As a consequence, in two dimensions the temporal scaling for the growth rate of the kinetic energy is unchanged $dE/dt \sim (Ag)^2 t$, but the viscous scale η (such that $\delta u(\eta)\eta/\nu = 1$) grows in time as $\eta(t) \sim \nu^{5/8}(Ag)^{-1/4}t^{1/8}$ and the viscous dissipation rate decreases as $\varepsilon(t) \sim \nu(\delta u(\eta)/\eta)^2 \sim \nu^{1/2}Agt^{-1/2}$ [25]. At long times, in two dimensions the viscous dissipation is expected to become negligible, while in three dimensions it remains proportional to dE/dt [28].

The temporal evolution of the kinetic energy growth rates and viscous dissipation rates observed in our simulations are reported in figure 6*a*. In the three-dimensional case at long times,
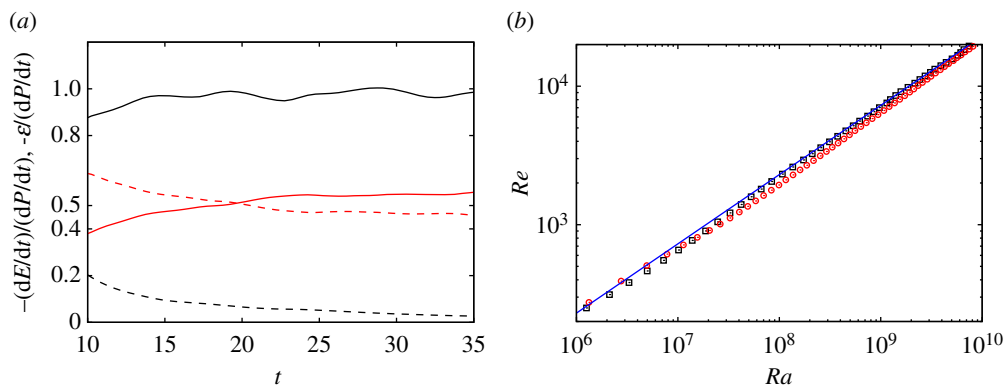
8

royalsocietypublishing.org/journal/rsta   Phil. Trans. R. Soc. A **380**: 20210084

Figure 6. (*a*) Temporal evolution of the kinetic energy growth rate $\mathrm{d}E/\mathrm{d}t$ (solid lines) and viscous dissipation rate ε (dashed lines) normalized with the power supplied $-\mathrm{d}P/\mathrm{d}t$ for the three-dimensional (red) and the two-dimensional (black) flows. (*b*) Reynolds number as a function of the Rayleigh number for the three-dimensional (red) and the two-dimensional (black) for the NS simulations. The blue line represents the dimensional scaling $Re \sim Ra^{1/2}$. (Online version in colour.)

almost 1/2 of the power supplied to the system contributes to the growth of the kinetic energy, while a similar fraction is dissipated by viscosity. This can be seen as a sort of equipartition between the two processes that occur in the ML: the growth of the kinetic energy of the plumes at large scale, which causes the growth of the extension of the ML, and the increase of the turbulent intensity at small scales, which causes the increase of the viscous dissipation as well as the homogenization of density fluctuations within the ML. As a consequence, in three dimensions, the two processes of mixing between the two reservoirs and between the plumes in the ML are always balanced. Conversely, in two dimensions, we observe a decay of the viscous dissipation (figure 6*a*), in agreement with the scaling predictions. The reduction of the intensity of small-scale turbulence with respect to the three-dimensional case results in a weaker small-scale eddy diffusivity, therefore the small-scale mixing is less efficient in two dimensions and the plumes remain more coherent and less homogenized than in three dimensions. The counterpart of this phenomenon is that, at long times, we find that in two dimensions almost all the potential energy is converted into kinetic energy (figure 6*a*). This causes the faster rate of growth of the ML in two dimensions (with respect to the three-dimensional case) at the expense of the reduced mixing efficiency within the ML.

The effects of the dimensionality on the RT system in porous media are qualitatively similar, but the physical mechanism which lies behind it is completely different. At variance with the turbulent case, here the dynamics is ruled by Darcy's Law and there are no differences in the physics of two-dimensional and three-dimensional systems. As shown in figure 1, in both cases, we observe the development of elongated fingers, which grows linearly in time in the vertical direction. Moreover, they undergo a complex, diffusive-like process in the horizontal direction, which is due to the broadening and merging of the fingers. This process is facilitated in three dimensions, because there are two lateral directions in which it can occur. Conversely, the lateral mixing is less efficient in a two-dimensional geometry. This explains why the fingers remains more coherent in two dimensions than in three dimensions (figure 5). Even though this process is completely different from that of the turbulent RT system, the outcome is similar. In three dimensions, the potential energy initially available in the system contributes both to the growth of the ML and the small-scale mixing. In two dimensions, the latter process is suppressed, while the first is enhanced.

Finally, we discuss the evolution of the Reynolds number in the case of RT bulk turbulence. This is defined in terms of the ML width h and the rms velocity u as $Re = uh/\nu$. The expected temporal scaling, both in two dimensions and in three dimensions, is $Re \sim t^3 \sim Ra^{1/2}$, as for the

Nusselt number. Figure 6*b* shows that this scaling is well reproduced over several orders of magnitude in both cases. At variance with the Nusselt number, which depends on the correlation between velocity and density fields, the dependence of *Re* on *Ra* displays almost no dependence on the dimensionality.

4. Conclusion

In this work, we investigate the dimensional effects in the case of two-dimensional and three-dimensional RT mixing in bulk flow and in porous media. The study is performed by means of numerical simulations of the transport equation for the density field, coupled within the Boussinesq approximation with the equation for the velocity field. In bulk flow, the velocity obeys the Navier–Stokes equation, while in porous media the dynamics is ruled by the Darcy equation. This leads to a completely different evolution of the two systems. Despite this difference, we have shown that the mixing properties of the NS and Darcy systems display a surprisingly similar dependence on the dimensionality. In particular, we have found that the mixing between the two reservoirs of the RT system is much faster (more than 50%) in two-dimensional geometry than in three-dimensional. We have quantified this effect by comparing the growth of the width *h* of the MLs in two dimensions and three dimensions. Moreover, at fixed extension *h*, the two-dimensional system displays larger correlations between the density and velocity fields, which results in a larger Nusselt number at the same Rayleigh number. The increased correlation is responsible for the faster growth of the ML. The counterpart of this phenomenon is that the density fluctuations within the ML are less homogenized in two dimensions than in three dimensions. This is shown by the variance of the density fluctuations in two dimensions, which is about 100% larger than in three dimensions. These effects are present both in the NS and Darcy cases, and they are quantitatively similar. At a qualitative level, they are already visible by comparing the convective structures of the two-dimensional and three-dimensional systems. At fixed time, the structures have longer vertical size in two dimensions than in three dimensions, and they are less blurred.

It is worth noting that our results are obtained in an ideal two-dimensional case, in which the confinement is not due to the presence of side walls. The presence of boundaries is expected to alter the dynamics of two-dimensional (or quasi-two-dimensional) systems, because the friction with the side walls dissipates part of the kinetic energy. This effect should be less relevant in the case of flows in porous media, in which the dynamics is dominated by the strong friction with the medium.

References

1. Frisch U, Lesieur M, Sulem PL. 1976 Crossover dimensions for fully developed turbulence. *Phys. Rev. Lett.* **37**, 895–897. (doi:10.1103/PhysRevLett.37.895)
2. Fournier JD, Frisch U. 1978 *d*-Dimensional turbulence. *Phys. Rev. A* **17**, 747–762. (doi:10.1103/PhysRevA.17.747)
3. Fournier J-D, Frisch U, Rose HA. 1978 Infinite-dimensional turbulence. *J. Phys. A. Math. Gen.* **11**, 187–198. (doi:10.1088/0305-4470/11/1/020)
4. Kraichnan RH. 1967 Inertial ranges in two-dimensional turbulence. *Phys. Fluids* **10**, 1417–1423. (doi:10.1063/1.1762301)
5. Frisch U. 1995 *Turbulence: the legacy of AN Kolmogorov*. Cambridge, UK: Cambridge Univ. Press.
6. Boffetta G, Ecke RE. 2012 Two-dimensional turbulence. *Annu. Rev. Fluid Mech.* **44**, 427–451. (doi:10.1146/fluid.2012.44.issue-1)

7. Smith LM, Chasnov JR, Waleffe F. 1996 Crossover from two- to three-dimensional turbulence. *Phys. Rev. Lett.* **77**, 2467–2470. (doi:10.1103/PhysRevLett.77.2467)

8. Celani A, Musacchio S, Vincenzi D. 2010 Turbulence in more than two and less than three dimensions. *Phys. Rev. Lett.* **104**, 184506. (doi:10.1103/PhysRevLett.104.184506)

9. Byrne D, Xia H, Shats M. 2011 Robust inverse energy cascade and turbulence structure in three dimensional layers of fluid. *Phys. Fluids* **23**, 095109. (doi:10.1063/1.3638620)

10. Xia H, Byrne D, Falkovich G, Shats M. 2011 Upscale energy transfer in thick turbulent fluid layers. *Nat. Phys.* **7**, 321–324. (doi:10.1038/nphys1910)

11. Alexakis A, Biferale L. 2018 Cascades and transitions in turbulent flows. *Phys. Rep.* **767–769**, 1–101. (doi:10.1016/j.physrep.2018.08.001)

12. Sharp DH. 1984 An overview of Rayleigh-Taylor instability. *Physica D* **12**, 3–18. (doi:10.1016/0167-2789(84)90510-4)

13. Boffetta G, Mazzino A. 2017 Incompressible Rayleigh-Taylor turbulence. *Annu. Rev. Fluid Mech.* **49**, 119–143. (doi:10.1146/fluid.2017.49.issue-1)

14. Cabot W, Cook A. 2006 Reynolds number effects on Rayleigh-Taylor instability with possible implications for type Ia supernovae. *Nat. Phys.* **2**, 562–568. (doi:10.1038/nphys361)

15. Takabe H, Mima K, Montierth L, Morse RL. 1985 Self-consistent growth rate of the Rayleigh-Taylor instability in an ablatively accelerating plasma. *Phys. Fluids* **28**, 3676–3682. (doi:10.1063/1.865099)

16. Sgattoni A, Sinigardi S, Fedeli L, Pegoraro F, Macchi A. 2015 Laser-driven Rayleigh-Taylor instability: plasmonic effects and three-dimensional structures. *Phys. Rev. E* **91**, 013106. (doi:10.1103/PhysRevE.91.013106)

17. Kilkenny J *et al.* 1994 A review of the ablative stabilization of the Rayleigh-Taylor instability in regimes relevant to inertial confinement fusion. *Phys. Plasmas* **1**, 1379–1389. (doi:10.1063/1.870688)

18. Saffman PG, Taylor G. 1954 The penetration of a fluid into a porous medium or Hele-Shaw cell containing a more viscous liquid. *Proc. R. Soc. Lond. A.* **245**, 312–329. (doi:10.1098/rspa.1958.0085)

19. Gopalakrishnan SS, Carballido-Landeira J, De Wit A, Knaepen B. 2017 Relative role of convective and diffusive mixing in the miscible Rayleigh-Taylor instability in porous media. *Phys. Rev. Fluids* **2**, 012501. (doi:10.1103/PhysRevFluids.2.012501)

20. De Paoli M, Zonta F, Soldati A. 2019 Rayleigh-Taylor convective dissolution in confined porous media. *Phys. Rev. Fluids* **4**, 023502. (doi:10.1103/PhysRevFluids.4.023502)

21. Nakanishi Y, Hyodo A, Wang L, Suekane T. 2016 Experimental study of 3D Rayleigh-Taylor convection between miscible fluids in a porous medium. *Adv. Water Res.* **97**, 224–232. (doi:10.1016/j.advwatres.2016.09.015)

22. Boffetta G, Borgnino M, Musacchio S. 2020 Scaling of Rayleigh-Taylor mixing in porous media. *Phys. Rev. Fluids* **5**, R062501. (doi:10.1103/PhysRevFluids.5.062501)

23. Huppert HE, Neufeld JA. 2014 The fluid mechanics of carbon dioxide sequestration. *Annu. Rev. Fluid Mech.* **46**, 255–272. (doi:10.1146/fluid.2013.46.issue-1)

24. Emami-Meybodi H, Hassanzadeh H, Green CP, Ennis-King J. 2015 Convective dissolution of CO_2 in saline aquifers: progress in modeling and experiments. *Int. J. Greenh. Gas Control* **40**, 238–266. (doi:10.1016/j.ijggc.2015.04.003)

25. Chertkov M. 2003 Phenomenology of Rayleigh-Taylor turbulence. *Phys. Rev. Lett.* **91**, 115001. (doi:10.1103/PhysRevLett.91.115001)

26. Boffetta G, Mazzino A, Musacchio S, Vozella L. 2009 Kolmogorov scaling and intermittency in Rayleigh-Taylor turbulence. *Phys. Rev. E* **79**, 065301. (doi:10.1103/PhysRevE.79.065301)

27. Celani A, Mazzino A, Vozella L. 2006 Rayleigh-Taylor turbulence in two dimensions. *Phys. Rev. Lett.* **96**, 134504. (doi:10.1103/PhysRevLett.96.134504)

28. Boffetta G, De Lillo F, Mazzino A, Musacchio S. 2012 Bolgiano scale in confined Rayleigh-Taylor turbulence. *J. Fluid Mech.* **690**, 426–440. (doi:10.1017/jfm.2011.446)

29. Borgnino M, Boffetta G, Musacchio S. 2021 Dimensional transition in Darcy-Rayleigh-Taylor mixing. *Phys. Rev. Fluids* **6**, 074501. (doi:10.1103/PhysRevFluids.6.074501)

30. Dalziel SB, Linden PF, Youngs DL. 1999 Self-similarity and internal structure of turbulence induced by Rayleigh-Taylor instability. *J. Fluid Mech.* **399**, 1–48. (doi:10.1017/S002211209900614X)